Geosci. Model Dev. Discuss., https://doi.org/10.5194/gmd-2019-15
Manuscript under review for journal Geosci. Model Dev.
Discussion started: 26 February 2019


Geoscientific Model Development Discussions
Open Access

# Developing a monthly albedo change radiative forcing kernel from satellite climatologies of Earth's shortwave radiation budget: CACK v1.0

Ryan M. Bright[1*] and Thomas L. O'Halloran[2,3]

1 – Norwegian Institute of Bioeconomy Research, Ås, Norway

2 – Department of Forest Resources and Environmental Conservation, Clemson University, Clemson, South Carolina, USA.

3 – Baruch Institute of Coastal Ecology and Forest Science, Clemson University, Georgetown, South Carolina, USA

[*]Contact: ryan.bright@nibio.no

## Abstract

Due to the potential for land use / land cover change (LULCC) to alter surface albedo, there is need within the LULCC science community for simple and transparent tools for predicting radiative forcings ( $\Delta F$ ) from surface albedo changes ( $\Delta\alpha_s$ ). To that end, the radiative kernel technique – developed by the climate modeling community to diagnose internal feedbacks within general circulation models (GCMs) – has been adopted by the LULCC science community as a tool to perform offline $\Delta F$ calculations for $\Delta\alpha_s$ . However, the GCM codes are not readily transparent and the atmospheric state variables used as model input are limited to single years, thus being sensitive to anomalous weather conditions that may have occurred in those simulated years. Observation-based kernels founded on longer-term climatologies of Earth's atmospheric state offer an attractive alternative to GCM-based kernels and could be updated annually at relatively low costs. Here, we evaluate simplified models of shortwave radiative transfer as candidates for an albedo change kernel founded on the Clouds and the

Geosci. Model Dev. Discuss., https://doi.org/10.5194/gmd-2019-15
Manuscript under review for journal Geosci. Model Dev.
Discussion started: 26 February 2019


Earth's Radiant Energy System (CERES) Energy Balance and Filled (EBAF) products. We find that a new, simple model supported by statistical analyses gives remarkable agreement when benchmarked to the mean of four GCM kernels and to two GCM kernels following emulation with their own boundary fluxes as input. Our findings lend support to its candidacy as a satellite-based alternative to GCM kernels and to its application in land-climate studies.

## 1. Introduction

Diagnosing changes to the shortwave radiation balance at the top-of-the-atmosphere (TOA) resulting from changes to albedo at the surface ($\Delta\alpha_s$) is an important step in predicting climate change. However, outside the climate science community, many researchers do not have the tools to convert $\Delta\alpha$ to the climate-relevant $\Delta F$ measure (Bright, 2015;Jones et al., 2015), which requires a detailed representation of the atmospheric constituents that absorb or scatter solar radiation (e.g. cloud, aerosols, and gases) and a sophisticated radiative transfer code. For single points in space or for small regions, these calculations are typically performed offline – meaning without feedbacks to the atmosphere (e.g., (Randerson et al. 2006)). Large-scale investigations (e.g. Amazonian or pan-boreal LULCC (Dickinson and Henderson-Sellers, 1988;Bonan et al., 1992)) typically prescribe the land surface layer in a GCM with initial and perturbed states, allowing the radiative transfer code to interact with the rest of the model. While this has the benefit of allowing interaction and feedbacks between surface albedo and scattering or absorbing components of the model, such an approach is computationally expensive and thereby restricts the number of LULCC scenarios that can be investigated (Atwood et al., 2016). Consequently, this method does not meet the needs of some modern LULCC studies which may require millions of individual land cover transitions to be evaluated cost effectively (Lutz and Howarth, 2015;Ghimire et al., 2014).

Geosci. Model Dev. Discuss., https://doi.org/10.5194/gmd-2019-15
Manuscript under review for journal Geosci. Model Dev.
Discussion started: 26 February 2019




Within the LULCC science community, two methods have primarily met the need for efficient $\Delta F$ calculations from $\Delta\alpha_s$: simplified parameterizations of atmospheric transfer of shortwave radiation (Bright and Kvalevåg, 2013;Cherubini et al., 2012;Bozzi et al., 2015;Muñoz et al., 2010;Caiazzo et al., 2014;Carrer et al., 2018), and radiative kernels (Ghimire et al., 2014;O'Halloran et al., 2012;Vanderhoof et al., 2013) derived from sophisticated radiative transfer schemes embedded in GCMs (Soden et al., 2008;Shell et al., 2008;Pendergrass et al., 2018;Block and Mauritsen, 2014). Simplified parameterizations of the LULCC science community have not been evaluated comprehensively in space and time. Bright & Kvalevåg (2013) evaluated the shortwave $\Delta F$ parameterization of Cherubini *et al.* (2012) when applied at several sites distributed globally on land, finding inconsistencies in performance at individual sites despite good overall cross-site performance. Radiative kernels (Soden et al., 2008;Shell et al., 2008;Pendergrass et al., 2018;Block and Mauritsen, 2014;Smith et al.) – while being based on state-of-the-art models of radiative transfer – have the downside of being model-dependent and not readily transparent. While the radiative transfer codes behind them are well-documented, the scattering components (i.e. aerosols, gases, and clouds) affecting transmission have many simplifying parameterizations, vary widely across models, and may contain significant biases (Dolinar et al., 2015;Wang and Su, 2013). An additional downside is the that atmospheric state variables used as model input are limited to single years, thus being sensitive to anomalous weather conditions that may have occurred in those years. Further, the application of a state-dependent GCM kernel may be undesirable in regions undergoing rapid changes in cloud cover or aerosol optical depth, such as in the northwest United States (Free and Sun, 2014) and in southern and eastern Asia (Zhao et al., 2018;Srivastava, 2017), respectively. A kernel based on remotely-sensed observations could be updated annually to capture changes in atmospheric state at relatively low costs.

Within the atmospheric science community, simplified radiative transfer frameworks have been developed, either to diagnose effective surface and atmospheric optical properties from climate model outputs, or to study the relative contributions of changes to these properties on shortwave flux changes at the top and bottom of the atmosphere (Rasool and Schneider, 1971;Winton, 2005;Winton, 2006;Taylor et al., 2007;Donohoe and Battisti, 2011;Atwood et al., 2016;Kashimura et al., 2017;Qu and Hall, 2006). These frameworks differ by whether or not the reflection and transmission properties of the atmospheric layer are assumed to have a directional dependency (Stephens et al., 2015) and by the number of variables required as input (Qu and Hall, 2006). Winton (2005) presented a four-parameter optical model to account for the directional dependency of up- and downwelling shortwave fluxes through a one-layer atmosphere and found good agreement (RMSE < 2% globally) when benchmarked to online radiative transfer calculations. Also considering a directional dependency of the atmospheric optical properties, Taylor et al. (2007) presented a two-parameter model where atmospheric absorption was assumed to occur at a level above atmospheric reflection. Donohoe and Battisti (2011) subsequently relaxed the directional dependency assumption and found the atmospheric attenuation of the surface albedo contribution to planetary albedo to be 8% higher than the model of Taylor et al. (2007). Elsewhere, Qu & Hall (2006) developed a framework making use of additional known atmospheric properties such as cloud cover fraction, cloud optical thickness, and the clear-sky planetary albedo which proved highly accurate when model estimates of planetary albedo were evaluated against climate models and satellite-based datasets.

Here, our primary research objective is to thoroughly evaluate a variety of shortwave kernels derived both analytically and statistically from satellite-based climatologies of Earth's shortwave radiation budget. To this end, we employ a 16-yr. time series of Earth's monthly mean radiation budget at both TOA (Loeb et al., 2017) and at the surface (Kato et al., 2012) as input to simplified models linking $\Delta\alpha_s$ to changes in the outgoing shortwave radiation flux at TOA. An initial performance screening is implemented where the six observation-driven kernels are first assessed both qualitatively and quantitatively against the mean of four GCM kernels (Shell et al., 2008;Soden et al., 2008;Pendergrass et al., 2018;Block and Mauritsen, 2014). Top performers are then subjected to a more rigorous evaluation where they are applied to emulate the GCM kernels using the GCM's own boundary fluxes as input, which eliminates any bias related to differences in the GCM representation of clouds or other atmosphere state variables. Our results elucidate the merits and uncertainties of empirical alternatives to those based on GCMs.

We start in Section 2 by introducing the satellite-based energy balance product and the variables derived from them utilized in this study. We then provide a brief overview of the GCM-based kernels and of the methods currently being applied within the LULCC science community to estimate instantaneous radiative forcings from surface albedo change. Section 3 details the methods applied to derive candidate GCM kernel alternatives from the radiative fluxes at Earth's upper and lower boundaries. We then present results of a comparative analysis in Section 4 and conclude with a brief discussion surrounding the merits and uncertainties of albedo change kernels based on satellite remote sensing.

## 2 Review of existing approaches

The NASA Clouds and the Earth's Radiant Energy System (CERES) Energy Balance and Filled (EBAF) products provide the monthly mean boundary fluxes and atmospheric state information necessary to derive our GCM kernel alternatives (CERES Science Team, 2018a, b). The latest EBAF-TOA Ed4.0 (version 4.0) products have many improvements with respect to the previous version (version 2.8, Loeb et al. 2009), including the use of advanced

Geosci. Model Dev. Discuss., https://doi.org/10.5194/gmd-2019-15
Manuscript under review for journal Geosci. Model Dev.
Discussion started: 26 February 2019

Geoscientific Model Development Discussions
Open Access EGU

and more consistent input data, retrieval of cloud properties, and instrument calibration (Loeb et al. 2018). The temporal extent of the EBAF dataset employed in our analysis spans the sixteen full calendar years from January 1, 2001 to December 31, 2016 (retrieved April, 2018). An overview of all CERES inputs used in our analysis is presented in Table 1.

< Table 1 >

*a. Shortwave* $\Delta F$ from $\Delta\alpha_s$

Earth's energy balance (at TOA) in an equilibrium state can be written:

$$0 = F = LW_{\uparrow}^{TOA} - (SW_{\downarrow}^{TOA} - SW_{\uparrow}^{TOA}) \quad (1)$$

where the equilibrium flux $F$ is a balance between the net solar energy inputs ($SW_{\downarrow}^{TOA} - SW_{\uparrow}^{TOA}$) and thermal energy output ($LW_{\uparrow}^{TOA}$). Perturbing this balance results in a radiative forcing *ΔF*, while perturbing the shortwave component is referred to as a shortwave radiative forcing and may be written as:

$$\Delta F = \Delta(SW_{\downarrow}^{TOA} - SW_{\uparrow}^{TOA}) = \Delta SW_{\downarrow}^{TOA}\left(1 - \frac{SW_{\uparrow}^{TOA}}{SW_{\downarrow}^{TOA}}\right) - SW_{\downarrow}^{TOA}\left(\Delta\frac{SW_{\uparrow}^{TOA}}{SW_{\downarrow}^{TOA}}\right) \quad (2)$$

where the shortwave radiative forcing results either from changes to solar energy inputs ($\Delta SW_{\downarrow}^{TOA}$) or from internal perturbations within the Earth system ($\Delta\frac{SW_{\uparrow}^{TOA}}{SW_{\downarrow}^{TOA}}$). The latter can be brought about by changes to the reflective properties of Earth's surface and/or atmosphere which is the focus in this paper.

*b. GCM-based radiative kernels*

Geosci. Model Dev. Discuss., https://doi.org/10.5194/gmd-2019-15
Manuscript under review for journal Geosci. Model Dev.
Discussion started: 26 February 2019


Geoscientific Model Development
Discussions
Open Access

The radiative kernel technique was developed as a way to assess various climate feedbacks from climate change simulations across multiple climate models in a computationally efficient manner (Shell et al., 2008;Soden et al., 2008). A radiative kernel is defined as the differential response of an outgoing radiation flux at TOA to an incremental change in some climate feedback variable -- such as water vapor, air temperature, or surface albedo (Soden et al., 2008). To generate a radiative kernel for a change in surface albedo $\Delta\alpha$ with a GCM, the prescribed surface albedo is perturbed incrementally by 1% and the response by $SW_{\uparrow}^{TOA}$ is recorded, which can be expressed as:

$$\Delta SW_{\uparrow}^{TOA} = SW_{\uparrow}^{TOA}(\alpha_s + \Delta\alpha_s) - SW_{\uparrow}^{TOA}(\alpha_s) = \frac{\partial SW_{\uparrow}^{TOA}}{\partial \alpha_s}\Delta\alpha \equiv K_{\alpha}\Delta\alpha_s \quad (3)$$

where $K_{\alpha}$ is the radiative kernel (in $Wm^{-2}$). The albedo change kernel can then be used with Eq. (1) to estimate an instantaneous shortwave radiative forcing ($\Delta F$) at TOA:

$$\begin{aligned} F + \Delta F &= LW_{\uparrow}^{TOA} - (SW_{\downarrow}^{TOA} - SW_{\uparrow}^{TOA} + K_{\alpha_s}\Delta\alpha) \\ \Delta F &= -K_{\alpha_s}\Delta\alpha \end{aligned} \quad (4)$$

*c. Simple kernel parameterizations of the LULCC science community*

Two simplified parameterizations of shortwave radiative transfer have been applied within the LULCC science community for estimating $\Delta F$ from $\Delta\alpha_s$ (Muñoz et al., 2010;Lutz et al., 2015;Bozzi et al., 2015;Caiazzo et al., 2014;Cherubini et al., 2012;Carrer et al., 2018). At the core of these parameterizations is the fundamental assumption that radiative transfer is wholly independent of (or unaffected by) $\Delta\alpha_s$. In other words, they neglect the change in the attenuating effect of multiple reflections between the surface and the atmosphere that accompanies a surface albedo change. Although not referred to as "kernels" in the literature, we present them as such to ensure consistency in notation and terminology henceforth. These are subsequently included in the kernel evaluation exercise presented in Section 4.

Geosci. Model Dev. Discuss., https://doi.org/10.5194/gmd-2019-15
Manuscript under review for journal Geosci. Model Dev.
Discussion started: 26 February 2019


Geoscientific Model Development Discussions
Open Access

The first simplified kernel presented in Muñoz et al. (2010) makes use of a local two-way transmittance factor based on the local clearness index (defined in Table 1):

$$\frac{\partial SW_{\uparrow}^{TOA}}{\partial \alpha_s}\Delta\alpha_s \equiv K_{\alpha}^{M10}\Delta\alpha_s = SW_{\downarrow}^{TOA}T^2\Delta\alpha_s \tag{5}$$

where $SW_{\downarrow}^{TOA}$ is the local incoming solar flux at TOA, $T$ is the local clearness index, and $\partial SW_{\uparrow}^{TOA}/\partial\alpha$ is the approximated change in the upwelling shortwave flux at TOA due to a change in albedo at the surface.

The second simplified kernel proposed in Cherubini et al. (2012) makes direct use of the solar flux incident at the surface $SW_{\downarrow}^{SFC}$ combined with a one-way transmission constant $k$:

$$\frac{\partial SW_{\uparrow}^{TOA}}{\partial \alpha_s}\Delta\alpha_s \equiv K_{\alpha}^{C12}\Delta\alpha_s = SW_{\downarrow}^{SFC}k\Delta\alpha_s \tag{6}$$

where $k$ is based on the global annual mean share of surface reflected shortwave radiation exiting a clear-sky (Lacis and Hansen, 1974;Lenton and Vaughan, 2009) and is hence temporally and spatially invariant. This value – or 0.85 -- is similar to the global mean ratio of forward-to-total shortwave scattering reported in Iqbal (1983). Bright & Kvalevåg (2013) evaluated Eq. (6) at several locations and found large biases for some regions and months, despite good overall performance globally (normalized RMSE = 7%; n = 120 months).

## 3. Methods

Simple analytical models developed by the climate science community treat the atmosphere as a single layer having various optical properties. These models vary by the number and type of optical properties included, whether these have a directional dependency (i.e., isotropic or anisotropic), or whether inputs other than those derived from the boundary fluxes are required (i.e., cloud properties). These models are adapted here to derive kernels analytically for $\Delta\alpha_s$.

*a. CERES isotropic kernel*

The surface contribution to the outgoing shortwave flux at TOA $SW_{\uparrow,SFC}^{TOA}$ is given (Stephens et al., 2015;Donohoe and Battisti, 2011;Winton, 2005) as:

$$SW_{\uparrow,SFC}^{TOA} = SW_{\downarrow}^{TOA}\alpha_s \frac{(1-r-a)^2}{(1-r\alpha_s)} \quad (7)$$

where $r$ is a single pass atmospheric reflection coefficient, $a$ is a single pass atmospheric absorption coefficient, $SW_{\downarrow}^{TOA}$ is the extraterrestrial (downwelling) shortwave flux at TOA, and $\alpha_s$ is the surface albedo (defined in Table 1). The expression in the denominator of the righthand term represents a fraction attenuated by multiple reflections between the surface and the atmosphere. This model assumes that the atmospheric optical properties $r$ and $a$ are insensitive to the origin and direction of shortwave fluxes – or in other words – that they are isotropic.

The single-pass reflectance coefficient is calculated from the system boundary fluxes (Table 1) following Winton (2005) and Kashimura *et al.* (2017):

$$r = \frac{SW_{\downarrow}^{TOA} SW_{\uparrow}^{TOA} - SW_{\downarrow}^{SFC} SW_{\uparrow}^{SFC}}{SW_{\downarrow}^{TOA\,2} - SW_{\uparrow}^{SFC\,2}} \quad (8)$$

while the single-pass absorption coefficient $a$ is given as:

$$a = 1 - r - T(1-\alpha_s r) \quad (9)$$

Geosci. Model Dev. Discuss., https://doi.org/10.5194/gmd-2019-15
Manuscript under review for journal Geosci. Model Dev.
Discussion started: 26 February 2019


where $T$ is the clearness index defined in Table 1. Our interest is in quantifying the $SW_{\uparrow,SFC}^{TOA}$ response to an albedo perturbation at the surface – or the partial derivative of $SW_{\uparrow,SFC}^{TOA}$ with respect to $\alpha$ in Eq. (7):

$$\frac{\partial SW_{\uparrow}^{TOA}}{\partial \alpha_s}\Delta\alpha_s = K_{\alpha_s}^{ISO}\Delta\alpha_s = \frac{SW_{\downarrow}^{TOA}(1-r-a)^2}{(1-r\alpha_s)^2}\Delta\alpha_s \tag{10}$$

where $K_{\alpha_s}^{ISO}$ is referred to henceforth as the CERES isotropic kernel.

*b. CERES anisotropic kernel*

The second kernel makes use of three directionally-dependent (anisotropic) bulk optical properties $r_{\uparrow}$, $t_{\uparrow}$, and $t_{\downarrow}$, where the first is the atmospheric reflectivity to upwelling shortwave radiation and the latter two are the atmospheric transmission coefficients for upwelling and downwelling shortwave radiation, respectively (Winton, 2005). It is not possible to derive $r_{\uparrow}$ analytically from the CERES all-sky boundary fluxes; however, Winton (2005) provides an empirical formula relating upwelling reflectivity $r_{\uparrow}$ to the ratio of all-sky to clear-sky fluxes incident at surface:

$$r_{\uparrow} = 0.05 + 0.85\left(1 - \frac{SW_{\downarrow}^{SFC}}{SW_{\downarrow,CLR}^{SFC}}\right) \tag{11}$$

where $SW_{\downarrow,CLR}^{SFC}$ is the clear-sky shortwave flux incident at the surface.

Knowing $r_{\uparrow}$, we can then solve for the two remaining optical parameters needed to derive our kernel:

$$t_{\downarrow} = \frac{SW_{\downarrow}^{SFC} - r_{\uparrow}SW_{\uparrow}^{SFC}}{SW_{\downarrow}^{TOA}} \tag{11}$$

$$t_{\uparrow} = T_a - \left[ t_{\downarrow} - t_{\downarrow}(1 - r_{\uparrow}\alpha_s) \right] \tag{12}$$

where $T_a$ is the effective atmospheric transmittance (Table 1) of the earth system.

The anisotropic kernel $K_{\alpha_s}^{ANISO}$ can now be derived as:

$$\frac{\partial SW_{\uparrow}^{TOA}}{\partial \alpha_s}\Delta\alpha_s = K_{\alpha_s}^{ANISO}\Delta\alpha_s = \frac{SW_{\downarrow}^{TOA} t_{\downarrow} t_{\uparrow}}{(1 - r_{\uparrow}\alpha_s)^2}\Delta\alpha_s \tag{13}$$

*c. CERES auxiliary input kernel*

Qu and Hall (2006) developed an alternative analytical kernel to the two described above. The model makes use of auxiliary cloud property information commonly provided in satellite-based products of Earth's radiation budget – including CERES EBAF – such as cloud cover area fraction, cloud visible optical depth, and clear-sky planetary albedo. The model links all-sky and clear-sky effective atmospheric transmissivities of the earth system through a linear coefficient $k$ relating the logarithm of cloud visible optical depth to the effective all-sky atmospheric transmissivity:

$$k = \frac{(T_{a,CLR}) - (T_a)}{\ln(\tau + 1)} \tag{14}$$

where $T_{a,CLR}$ is the clear-sky effective system transmissivity, $T_a$ is the all-sky effective system transmissivity, and $\tau$ is the cloud visible optical depth. This linear coefficient can then be used together with the cloud cover area fraction to derive a shortwave kernel based on the model of Qu and Hall (2006) – or $K_{\alpha_s}^{QH06}$:

$$\frac{\partial SW_{\uparrow}^{TOA}}{\partial \alpha_s}\Delta\alpha_s = K_{\alpha_s}^{QH06}\Delta\alpha_s = SW_{\downarrow}^{SFC}\left[ (T_a) - kc\ln(\tau + 1) \right]\Delta\alpha_s \tag{15}$$

where $c$ is the cloud cover area fraction.

Geosci. Model Dev. Discuss., https://doi.org/10.5194/gmd-2019-15
Manuscript under review for journal Geosci. Model Dev.
Discussion started: 26 February 2019

Geoscientific Model Development Discussions
Open Access EGU

*d. CERES statistical kernel*

To determine whether the GCM-based kernels could be approximated with sufficient fidelity using even simpler model formulations based on the CERES boundary data, we applied machine learning to identify potential model forms using the CERES EBAF all-sky boundary fluxes (or system parameters derived from these fluxes) that minimized the sum of squared residuals between monthly means of four GCM-based kernels (described below) and model estimates. The reference dataset consisted of a random global sample of 50,000 (~50%) 2.8° x 2.8° grid cells, from the multi-GMC mean, of which 50% were used for training and 50% for validation. Models were identified using a form of genetic programming known as symbolic regression (Eureqa®; Nutonian Inc.; (Schmidt and Lipson, 2009, 2010)) which searches for both optimal model structure and coefficients. A parsimonious solution was chosen by minimizing the error metric and model complexity using the Pareto front (Smits and Kotanchek, 2005). Based on the mean squared deviation (MSD) and Akaike's information criterion (AIC), the best model form of the statistical kernel – subsequently referred to as $K_{\alpha_s}^{BO18}$ -- is given as:

$$\frac{\partial SW_{\uparrow}^{TOA}}{\partial \alpha_s}\Delta\alpha_s = K_{\alpha_s}^{BO18}\Delta\alpha_s = SW_{\downarrow}^{SFC}\sqrt{T}\Delta\alpha_s \tag{16}$$

*d. Initial screening of candidate models for a CERES-based kernel*

Four GCM kernels are employed as benchmarks to initially screen the six CERES-based kernel model candidates: the Community Atmosphere Model version 3, or CAM3 (Shell et al., 2008), the Community Atmosphere Model version 5, or CAM5 (Pendergrass et al., 2018), the European Center and Hamburg model version 6, or ECHAM6 (Block and Mauritsen, 2014), and the Geophysical Fluid Dynamics Laboratory model version AM2p12b, or GFDL (Soden et al., 2008). The four GCM kernels vary in vertical and horizontal resolution, parameterization of shortwave radiative transfer, and year of atmospheric state (input variables).

We compute a skill metric analogous to the "relative error" metric used to evaluate GCMs by Anav et al. (2013) that takes into account error in the spatial pattern between a model and an observation. Because we have no true observational reference, our evaluation instead focuses on the disagreement or deviation between CERES and GCM kernels at the monthly time step. Given interannual climate variability in the earth system, the challenge of comparing the multi-year CERES kernel to a single-year GCM kernel can be partially overcome by averaging the four GCM kernels.

Using the multi-GCM mean as the reference, we first compute the absolute deviation $AD^{X}_{m,p}$ as:

$$AD^{X}_{m,p} = \left| CERES^{X}_{m,p} - \overline{GCM}_{m,p} \right| \tag{17}$$

where $CERES^{X}_{m,p}$ is the kernel for CERES model $X$ in month $m$ and pixel $p$ and $\overline{GCM}_{m,p}$ is the multi-GCM mean of the same pixel and month. $AD^{X}_{m,p}$ is then normalized to the maximum absolute deviation of all six CERES kernels for the same pixel and month to obtain a normalized absolute deviation, $NAD^{X}_{m,p}$, which is analogous to the "relative error" metric of Anav et al. (2013) with values ranging between 0 and 1:

$$NAD^{X}_{m,p} = 1 - \frac{AD^{X}_{m,p}}{\max(AD_{m,p})} \tag{18}$$

where $\max(AD_{m,p})$ is the maximum absolute deviation of all six CERES kernels at pixel $p$ and month $m$.

Geosci. Model Dev. Discuss., https://doi.org/10.5194/gmd-2019-15
Manuscript under review for journal Geosci. Model Dev.
Discussion started: 26 February 2019


Geoscientific Model Development Discussions
Open Access
EGU

CERES kernel ranking is based on the mean relative absolute deviation in both space and time – or $NAD^X$ :

$$NAD^X = \frac{1}{M}\sum_{m=1}^{M}\frac{1}{P}\sum_{p=1}^{P} NAD_{m,p}^X \tag{19}$$

where $M$ is the total number of months (i.e., 12) and $P$ is the total number of grid cells.

*e. GCM kernel emulation*

In order to eliminate any bias related to differences in the atmospheric state embedded in the GCM and CERES-derived kernels, we re-compute our simple kernels using the same shortwave boundary fluxes used to compute the two most recent albedo change kernels based on ECHAM6 (Block and Mauritsen, 2014) and CAM5 (Pendergrass et al., 2018). This enables a more critical evaluation of the functional form of the simple models in relation to the more sophisticated radiative transfer schemes employed by ECHAM6 (Stevens et al., 2013) and CAM5 (Hurrell et al., 2013).

## 4. Results

*a. Initial kernel performance screening*

Seasonally, differences in latitude band means between the CERES and multi-GCM mean kernels are shown in Figure 1.

< Figure 1 >

Geosci. Model Dev. Discuss., https://doi.org/10.5194/gmd-2019-15
Manuscript under review for journal Geosci. Model Dev.
Discussion started: 26 February 2019



Qualitatively, starting with December-January-February (*DJF*), $K_{\alpha}^{BO18}$ gives the best agreement with $K_{\alpha}^{\overline{GCM}}$ with the exception of the zone around 55 – 65°S (-55 – -65°), where $K_{\alpha}^{QH06}$ gives slightly better agreement (Fig. 1A). In March-April-May (*MAM*), $K_{\alpha}^{BO18}$ appears to give the best overall agreement with the exception of the high Arctic, where $K_{\alpha}^{ANISO}$ and $K_{\alpha}^{C12}$ give better agreement, and with the exception of the zone around 60 – 65°S (-60 – -65°) where $K_{\alpha}^{QH06}$, $K_{\alpha}^{ANISO}$, and $K_{\alpha}^{C12}$ agree best with $K_{\alpha}^{\overline{GCM}}$ (Fig. 1B). The largest spread in disagreement across all six CERES kernels is found in June-July-August (*JJA*; Fig. 1C) at northern high latitudes. $K_{\alpha}^{BO18}$ appears to agree best both here and elsewhere with the exception of the zone between ~20 – 35°N, where $K_{\alpha}^{QH06}$ gives slightly better agreement. In September-October-November (*SON*), $K_{\alpha}^{BO18}$ agrees best with $K_{\alpha}^{\overline{GCM}}$ at all latitudes except the zone between 10 – 25°N and 55 – 65°S where $K_{\alpha}^{QH06}$ agrees slightly better.

Quantitatively, the proportion of the total variance explained by linear regressions of monthly $K_{\alpha}^{\overline{GCM}}$ on monthly $K_{\alpha}^{CERES}$ (i.e., $R^2$) is highest and equal for the CERES kernels based on the ANISO, QH06, and BO18 models (Fig. 2 B, C, & D). Of these three, $K_{\alpha}^{QH06}$ has a y-intercept ($B_0$) closest to 0 and a slope (*m*) of 1, although the root mean squared deviation (*RMSD*) – an accuracy measure – is slightly better (lower) for $K_{\alpha}^{BO18}$. The two CERES kernels with the lowest $R^2$, highest slopes (negative deviations), highest *RMSD*s, and y-intercepts with the largest absolute difference from zero are those based on the ISO and M10 models (Fig. 2 A&E).

< Figure 2 >

Geosci. Model Dev. Discuss., https://doi.org/10.5194/gmd-2019-15
Manuscript under review for journal Geosci. Model Dev.
Discussion started: 26 February 2019


Although the y-intercept deviation from 0 for $K_{\alpha}^{C12}$ is relatively low, its *RMSD* is ~50% higher than that of $K_{\alpha}^{QH06}$, $K_{\alpha}^{BO18}$, and $K_{\alpha}^{ANISO}$ and leads to notable positive deviation from the multi-GCM mean ($K_{\alpha}^{\overline{GCM}}$) judging by its slope of 0.92.

*c. Normalized absolute deviation*

Globally, $NAD^{X}$ for the QH06, ANISO, and BO18 kernels are far superior to the ISO, M10, and C12 kernels (Table 2).

< Table 2 >

After filtering to remove grid cells for oceans and other water bodies, $NAD^{X}$ scores for these three kernels decreased; the decrease was smallest for $K_{\alpha}^{BO18}$ (-0.03) and largest for $K_{\alpha}^{QH06}$ (-0.06). Despite constraining the analysis to land surfaces only, the rank order remained unchanged (Table 2).

*d. GCM kernel emulation and additional performance screening*

Because the simple kernel based on the QH06 model ($K_{\alpha}^{QH06}$) required auxiliary inputs for cloud cover area fraction and cloud optical depth – two atmospheric state variables not provided with the ECHAM6 and CAM5 kernel datasets – it was not possible to emulate these two GCM kernels using the QH06 model. Additional performance evaluation through GCM kernel emulation is therefore restricted to the ANISO and BO18 models.

< Figure 3 >

Globally, the kernel based on the ANISO model displays larger annual mean biases relative to BO18 when compared to both ECHAM6 and CAM5 kernels (Figure 3). Notable positive biases over land with respect to both ECHAM6 and CAM5 kernels are evident in the northern Andes region of South America, the Tibetan plateau, and the tropical island region comprising Indonesia, Malaysia, and Papua New Guinea (Fig. 3 A & C). Notable negative biases over land with respect to both ECHAM6 and CAM5 kernels are evident over Greenland, Antarctica, northeastern Africa, and the Arabian Peninsula (Fig. 3 A & C).

< Figure 4 >

Globally, annual biases for BO18 are generally found to be lower than for ANISO and are mostly non-existent in extra-tropical ocean regions (Fig. 3 B & D). Patterns in biases over land are mostly negative with the exception of Saharan Africa where the annual mean bias with respect to both GCMs is positive. For BO18, systematic positive biases – or biases evident with respect to both GCM kernels – appear over eastern tropical and subtropical marine coastal upwelling zones where marine stratocumulus cloud dynamics are difficult for GCMs to resolve (Bretherton et al., 2004;Richter, 2015).

< Table 3 >

Performance metrics based on regressing monthly kernels from the two GCMs on kernels emulated with both ANISO and BO18 models indicate a greater overall accuracy (or agreement) for BO18 (Figure 4). RMSDs for monthly kernels emulated with BO18 are 9.0 and 8.2 W m$^{-2}$ with respect to CAM5 and ECHAM6, respectively – which is ~50-60% of the RMSDs emulated with the ANISO model. Focusing henceforth only on the kernel emulated with BO18 model, negative biases are evident in all months (Table 3), with the largest biases (in magnitude) appearing in May (-4.4 W m$^{-2}$) and November (-2.5 W m$^{-2}$) for CAM5 and ECHAM6, respectively. In absolute terms, largest biases of 8.6 W m$^{-2}$ and 6.8 W m$^{-2}$ appear in June for CAM5 and ECHAM6, respectively. Annually, the mean absolute bias for CAM5 and ECHAM6 is 6.8 and 6.1 W m$^{-2}$, respectively – a magnitude which seems remarkably low if one compares this to the annual mean disagreement (standard deviation) of 33 W m$^{-2}$ across all four GCM kernels (not shown).

## 5. Discussion and conclusions

Motivated by an increasing abundance of climate impact research focusing on land processes in recent years, we comprehensively evaluated six simplified models linking shortwave radiative flux perturbations at TOA with surface albedo changes at the surface. Relative to albedo change kernels based on sophisticated radiative transfer schemes embedded in GCMs, the simplified models evaluated here can be updated frequently at relatively low cost using boundary fluxes obtained from remote sensing-based products of Earth's shortwave energy budget. This allows greater flexibility to meet the needs of research that focuses on longer-term albedo trends or regions currently undergoing rapid change in atmospheric composition. Although some modeling groups have provided recent updates to radiative kernels using the latest GCM versions, the atmospheric state of the boundary conditions used to derive them may be considered outdated or not in sync with that required for some applications.

Based on both qualitative and quantitative benchmarking against the mean of four GCM kernels, the simple model derived from machine learning, BO18, together with the two analytically derived models, QH06 and ANISO, proved far superior to the M10, C12, and the ISO kernel models. When subjected to additional performance evaluation, however, we found that the BO18 model was able to more robustly emulate the ECHAM6 and CAM5 kernels with exceptionally high accuracy, suggesting that this model can serve as a suitable candidate for an albedo change kernel based on CERES boundary fluxes. The RMSD of this kernel – henceforth referred to as the CERES Albedo Change Kernel (CACK v1.0) – was found to be 6.8 and 6.1 W $m^{-2}$ when benchmarked to the CAM5 and ECHAM6 kernel, respectively – a magnitude which is only ~20% of the standard deviation found across four GCM kernels (annual mean). CACK's remarkable simplicity lends support to the idea of using machine learning to explore and detect emergent properties of shortwave radiative transfer in future research.

Despite the stronger empirical foundation of CACK over a GCM-based kernel, it is important to recognize its limitations. Firstly, the monthly CERES EBAF-Surface product used to define lower atmospheric boundary conditions is not strictly an observation. The space-borne observation platform is not able to directly observe Earth's surface fluxes under overcast conditions and hence requires model augmentation. However, the energy-balancing step ensures that fluxes are adjusted to match the observed rate of heat accumulation in the climate system (i.e., the oceans) (Hansen et al., 2005). These processes, as well as extensive ground validation and testing, are documented elsewhere (Kato et al., 2013;Loeb et al., 2009). Further, while CACK has a finer spatial resolution than most GCM kernels, it still represents a spatially averaged response rather than a truly local response; in other words, the state variables used to define the response are tied to the course spatial (i.e., 1° x 1°) resolution of the CERES EBAF product grids. Lastly, it is important to emphasize that CACK is based on the climate conditions of the present day (2001-2016); hence, caution should be exercised when applying it to estimate $\Delta F$ associated with albedo changes occurring outside this range.

To conclude, we evaluated six simplified albedo change kernels based on CERES shortwave boundary fluxes as candidate alternatives to GCM-based albedo change kernels. Albedo change kernels are useful tools for estimating instantaneous shortwave radiative forcings connected to anthropogenic land use activities. Our results showed that the BO18 model developed and presented in this study is the best candidate for a CERES albedo change kernel -- or CACK. CACK provides a higher spatial resolution, higher transparency alternative to existing kernels based on GCMs. CACK could be easily applied as part of Monitoring, Reporting, and Verification (MRV) frameworks for biogeophysical impacts on land, analogous to those which currently exist for land sector greenhouse gas emissions. Given the extensive time span of the CERES EBAF products, CACK based on a multi-year climatology of Earth's shortwave radiation budget would better-account for internal climate variability in the earth system. However, CACK's flexibility regarding input year should make it broadly appealing across a range of disciplines. One example is the land-based solar radiation management (SRM) research community who frequently calculate $\Delta F$ from $\Delta\alpha$ to evaluate climate mitigation strategies (Ridgwell et al., 2009;Seneviratne et al., 2018;Akbari et al., 2009).

**Code Availability**

An open source Octave (Eaton et al., 2018) script file for generating monthly CACK from CERES EBAF data and example input files are included as a Supplement. The script also demonstrates calculating a TOA RF from CACK and monthly surface albedo perturbation at a user-specified location.

**Data Availability**

CERES EBAF data are available for download at: https://ceres.larc.nasa.gov/products.php?product=EBAF-TOA . The CAM3 kernel is available at: http://people.oregonstate.edu/~shellk/kernel.html . The CAM5 kernel is available at: https://www.earthsystemgrid.org/ac/guest/secure/sso.html . The ECHAM5 kernel is available at: https://swiftbrowser.dkrz.de/public/dkrz_0c07783a-0bdc-4d5e-9f3b-c1b86fac060d/Radiative_kernels/ .

## Author contributions

T.L.O. conceptualized the study. R.M.B. and T.L.O. developed the methodology, curated the data, designed the computer programs, and carried out the formal analysis. R.M.B. wrote the original draft, and R.M.B. and T.O. reviewed and edited and final manuscript. T.L.O. produced the figures.

## Acknowledgements

R.M.B. was supported by the Research Council of Norway, grants #244074/E20 and #250113/F20; T.L.O. was supported by Climate and Land Use program award #2017-68002-26612 of the USDA National Institute of Food and Agriculture.

## References

Akbari, H., Menon, S., and Rosenfeld, A.: Global cooling: increasing world-wide urban albedos to offset CO2, Climatic Change, 94, 275-286, 2009.

Anav, A., Friedlingstein, P., Kidston, M., Bopp, L., Ciais, P., Cox, P., Jones, C., Jung, M., Myneni, R., and Zhu, Z.: Evaluating the Land and Ocean Components of the Global Carbon Cycle in the CMIP5 Earth System Models, Journal of Climate, 26, 6801-6843, 10.1175/JCLI-D-12-00417.1, 2013.

Atwood, A. R., Wu, E., Frierson, D. M. W., Battisti, D. S., and Sachs, J. P.: Quantifying Climate Forcings and Feedbacks over the Last Millennium in the CMIP5–PMIP3 Models, Journal of Climate, 29, 1161-1178, 10.1175/jcli-d-15-0063.1, 2016.

Block, K., and Mauritsen, T.: Forcing and feedback in the MPI-ESM-LR coupled model under abruptly quadrupled CO2, Journal of Advances in Modeling Earth Systems, 5, 676-691, 10.1002/jame.20041, 2014.

Bonan, G. B., Pollard, D., and Thompson, S. L.: Effects of Boreal Forest Vegetation on Global Climate, Nature, 359, 716-718, 1992.

Bozzi, E., Genesio, L., Toscano, P., Pieri, M., and Miglietta, F.: Mimicking biochar-albedo feedback in complex Mediterranean agricultural landscapes, Environmental Research Letters, 10, 084014, 2015.

Bretherton, C. S., Uttal, T., Fairall, C. W., Yuter, S. E., Weller, R. A., Baumgardner, D., Comstock, K., Wood, R., and Raga, G. B.: The Epic 2001 Stratocumulus Study, Bulletin of the American Meteorological Society, 85, 967-978, 10.1175/BAMS-85-7-967, 2004.

Bright, R. M., and Kvalevåg, M. M.: Technical note: Evaluating a simple parameterization of radiative shortwave forcing from surface albedo change, Atmospheric Chemistry and Physics, 13, 11169-11174, 2013.

Bright, R. M.: Metrics for Biogeophysical Climate Forcings from Land Use and Land Cover Changes and Their Inclusion in Life Cycle Assessment: A Critical Review, Environmental Science & Technology, 49, 3291-3303, 10.1021/es505465t, 2015.
Caiazzo, F., Malina, R., Staples, M. D., Wolfe, P., J. ,, Yim, S. H. L., and Barrett, S. R. H.: Quantifying the climate impacts of albedo changes due to biofuel production: a comparison with biogeochemical effects, Environmental Research Letters, 9, 024015, 2014.

Carrer, D., Pique, G., Ferlicoq, M., Ceamanos, X., and Ceschia, E.: What is the potential of cropland albedo management in the fight against global warming? A case study based on the use of cover crops, Environmental Research Letters, 13, 044030, 2018.

CERES Science Team: CERES EBAF-Surface Edition 4.0. NASA Atmospheric Science and Data Center (ASDC). https://doi.org/10.5067/TERRA+AQUA/CERES/EBAF-SURFACE_L3B004.0 . Accessed January 14, 2018., in, 2018a.

CERES Science Team: CERES EBAF-TOA Edition 4.0. NASA Atmospheric Science and Data Center (ASDC). https://doi.org/10.5067/TERRA+AQUA/CERES/EBAF-TOA_L3B004.0 . Accessed January 14, 2018. , in, 2018b.

Cherubini, F., Bright, R. M., and Strømman, A. H.: Site-specific global warming potentials of biogenic CO2 for bioenergy: contributions from carbon fluxes and albedo dynamics, Environmental Research Letters, 7, 045902, 2012.

Dickinson, R. E., and Henderson-Sellers, A.: Modelling tropical deforestation: A study of GCM land-surface parametrizations, Quarterly Journal of the Royal Meteorological Society, 114, 439-462, 10.1002/qj.49711448009, 1988.

Dolinar, E. K., Dong, X., Xi, B., Jiang, J. H., and Su, H.: Evaluation of CMIP5 simulated clouds and TOA radiation budgets using NASA satellite observations, Clim. Dyn., 44, 2229-2247, 10.1007/s00382-014-2158-9, 2015.

Donohoe, A., and Battisti, D. S.: Atmospheric and Surface Contributions to Planetary Albedo, Journal of Climate, 24, 4402-4418, 10.1175/2011JCLI3946.1, 2011.

Eaton, J.W., Bateman, D., Hauberg, S., and Wehbring, R. (2018). GNU Octave version 4.4.1 manual: a high-level interactive language for numerical computations. https://www.gnu.org/software/octave/doc/v4.4.1/

Free, M., and Sun, B.: Trends in U.S. Total Cloud Cover from a Homogeneity-Adjusted Dataset, Journal of Climate, 27, 4959-4969, 10.1175/jcli-d-13-00722.1, 2014.

Ghimire, B., Williams, C. A., Masek, J., Gao, F., Wang, Z., Schaaf, C., and He, T.: Global albedo change and radiative cooling from anthropogenic land cover change, 1700 to 2005 based on MODIS, land use harmonization, radiative kernels, and reanalysis, Geophysical Research Letters, 41, 9087-9096, 10.1002/2014GL061671, 2014.

Hansen, J., Nazarenko, L., Ruedy, R., Sato, M., Willis, J., Del Genio, A., Koch, D., Lacis, A., Lo, K., and Menon, S.: Earth's energy imbalance: Confirmation and implications, Science, 308, 1431-1435, 2005.

Hurrell, J. W., Holland, M. M., Gent, P. R., Ghan, S., Kay, J. E., Kushner, P. J., Lamarque, J. F., Large, W. G., Lawrence, D., Lindsay, K., Lipscomb, W. H., Long, M. C., Mahowald, N., Marsh, D. R., Neale, R. B., Rasch, P., Vavrus, S., Vertenstein, M., Bader, D., Collins, W. D., Hack, J. J., Kiehl, J., and Marshall, S.: The Community Earth System Model: A Framework for Collaborative Research, Bulletin of the American Meteorological Society, 94, 1339-1360, 10.1175/BAMS-D-12-00121.1, 2013.

Iqbal, M.: An introduction to solar radiation, Academic Press Canada, Ontario, CA, 389 pp., 1983.

Jones, A. D., Calvin, K. V., Collins, W. D., and Edmonds, J.: Accounting for radiative forcing from albedo change in future global land-use scenarios, Climatic Change, 131, 691-703, 10.1007/s10584-015-1411-5, 2015.
Kashimura, H., Abe, M., Watanabe, S., Sekiya, T., Ji, D., Moore, J. C., Cole, J. N. S., and Kravitz, B.: Shortwave radiative forcing, rapid adjustment, and feedback to the surface by sulfate geoengineering: analysis of the Geoengineering Model Intercomparison Project G4 scenario, Atmos. Chem. Phys., 17, 3339-3356, 2017.

Kato, S., Loeb, N. G., Rose, F. G., Doelling, D. R., Rutan, D. A., Caldwell, T. E., Yu, L., and Weller, R. A.: Surface Irradiances Consistent with CERES-Derived Top-of-Atmosphere Shortwave and Longwave Irradiances, Journal of Climate, 26, 2719-2740, 10.1175/JCLI-D-12-00436.1, 2012.

Kato, S., Loeb, N. G., Rose, F. G., Doelling, D. R., Rutan, D. A., Caldwell, T. E., Yu, L., and Weller, R. A.: Surface irradiances consistent with CERES-derived top-of-atmosphere shortwave and longwave irradiances, Journal of Climate, 26, 2719-2740, 2013.

Lacis, A. A., and Hansen, J. E.: A parameterization for the absorption of solar radiation in the earth's atmosphere, Journal of Atmospheric Sciences, 31, 118-133, 1974.

Lenton, T. M., and Vaughan, N. E.: The radiative forcing potential of different climate geoengineering options, Atmospheric Chemistry and Physics 9, 5539-5561, 2009.

Loeb, N. G., Wielicki, B. A., Doelling, D. R., Smith, G. L., Keyes, D. F., Kato, S., Manalo-Smith, N., and Wong, T.: Toward optimal closure of the Earth's top-of-atmosphere radiation budget, Journal of Climate, 22, 748-766, 2009.

Loeb, N. G., Doelling, D. R., Wang, H., Su, W., Nguyen, C., Corbett, J. G., Liang, L., Mitrescu, C., Rose, F. G., and Kato, S.: Clouds and the Earth's Radiant Energy System (CERES) Energy Balanced and Filled (EBAF) Top-of-Atmosphere (TOA) Edition-4.0 Data Product, Journal of Climate, 31, 895-918, 10.1175/JCLI-D-17-0208.1, 2017.

Lutz, D. A., Burakowski, E. A., Murphy, M. B., Borsuk, M. E., Niemiec, R. M., and Howarth, R. B.: Tradeoffs between three forest ecosystem services across the state of New Hampshire, USA: timber, carbon, and albedo, Ecological Applications, 26, 146-161, 10.1890/14-2207.1, 2015.

Lutz, D. A., and Howarth, R. B.: The price of snow: albedo valuation and a case study for forest management, Environmental Research Letters, 10, 064013, 2015.

Muñoz, I., Campra, P., and Fernández-Alba, A. R.: Including CO2-emission equivalence of changes in land surface albedo in life cycle assessment. Methodology and case study on greenhouse agriculture, International Journal of Life Cycle Assessment, 15, 672-681, 2010.

O'Halloran, T. L., Law, B. E., Goulden, M. L., Wang, Z., Barr, J. G., Schaaf, C., Brown, M., Fuentes, J. D., Göckede, M., Black, A., and Engel, V.: Radiative forcing of natural forest disturbances, Global Change Biology, 18, 555-565, 2012.

Pendergrass, A. G., Conley, A., and Vitt, F. M.: Surface and top-of-atmosphere radiative feedback kernels for CESM-CAM5, Earth Syst. Sci. Data, 10, 317-324, 10.5194/essd-10-317-2018, 2018.

Qu, X., and Hall, A.: Assessing Snow Albedo Feedback in Simulated Climate Change, Journal of Climate, 19, 2617-2630, 10.1175/JCLI3750.1, 2006.

Rasool, S. I., and Schneider, S. H.: Atmospheric Carbon Dioxide and Aerosols: Effects of Large Increases on Global Climate, Science, 173, 138-141, 10.1126/science.173.3992.138, 1971.

Richter, I.: Climate model biases in the eastern tropical oceans: causes, impacts and ways forward, Wiley Interdisciplinary Reviews: Climate Change, 6, 345-358, 10.1002/wcc.338, 2015.

Ridgwell, A., Singarayer, J. S., Hetherington, A. M., and Valdes, P. J.: Tackling regional climate change by leaf albedo bio-geoengineering, Current Biology, 19, 146-150, 2009.

Schmidt, M., and Lipson, H.: Distilling free-form natural laws from experimental data, science, 324, 81-85, 2009.

Schmidt, M., and Lipson, H.: Symbolic regression of implicit equations, in: Genetic Programming Theory and Practice VII, Springer, 73-85, 2010.

Seneviratne, S. I., Phipps, S. J., Pitman, A. J., Hirsch, A. L., Davin, E. L., Donat, M. G., Hirschi, M., Lenton, A., Wilhelm, M., and Kravitz, B.: Land radiative management as contributor to regional-scale climate adaptation and mitigation, Nature Geoscience, 11, 88-96, 10.1038/s41561-017-0057-5, 2018.

Shell, K. M., Kiehl, J. T., and Shields, C. A.: Using the Radiative Kernel Technique to Calculate Climate Feedbacks in NCAR's Community Atmospheric Model, Journal of Climate, 21, 2269-2282, 10.1175/2007JCLI2044.1, 2008.

Smith, C. J., Kramer, R. J., Myhre, G., Forster, P. M., Soden, B. J., Andrews, T., Boucher, O., Faluvegi, G., Fläschner, D., Hodnebrog, Ø., Kasoar, M., Kharin, V., Kirkevåg, A., Lamarque, J.-F., Mülmenstädt, J., Olivié, D., Richardson, T., Samset, B. H., Shindell, D., Stier, P., Takemura, T., Voulgarakis, A., and Watson-Parris, D.: Understanding Rapid Adjustments to Diverse Forcing Agents, Geophysical Research Letters, 0, doi:10.1029/2018GL079826.

Smits, G. F., and Kotanchek, M.: Pareto-front exploitation in symbolic regression, in: Genetic programming theory and practice II, Springer, 283-299, 2005.

Soden, B. J., Held, I. M., Colman, R., Shell, K. M., Kiehl, J. T., and Shields, C. A.: Quantifying Climate Feedbacks Using Radiative Kernels, Journal of Climate, 21, 3504-3520, 10.1175/2007JCLI2110.1, 2008.

Srivastava, R.: Trends in aerosol optical properties over South Asia, International Journal of Climatology, 37, 371-380, doi:10.1002/joc.4710, 2017.

Stephens, G. L., O'Brien, D., Webster, P. J., Pilewski, P., Kato, S., and Li, J.-l.: The albedo of Earth, Reviews of Geophysics, 53, 141-163, 10.1002/2014RG000449, 2015.

Stevens, B., Giorgetta, M., Esch, M., Mauritsen, T., Crueger, T., Rast, S., Salzmann, M., Schmidt, H., Bader, J., Block, K., Brokopf, R., Fast, I., Kinne, S., Kornblueh, L., Lohmann, U., Pincus, R., Reichler, T., and Roeckner, E.: Atmospheric component of the MPI-M Earth System Model: ECHAM6, Journal of Advances in Modeling Earth Systems, 5, 146-172, doi:10.1002/jame.20015, 2013.

Taylor, K. E., Crucifix, M., Braconnot, P., Hewitt, C. D., Doutriaux, C., Broccoli, A. J., Mitchell, J. F. B., and Webb, M. J.: Estimating Shortwave Radiative Forcing and Response in Climate Models, Journal of Climate, 20, 2530-2543, 10.1175/JCLI4143.1, 2007.

Vanderhoof, M., Williams, C. A., Ghimire, B., and Rogan, J.: Impact of mountain pine beetle outbreaks on forest albedo and radiative forcing, as derived from Moderate Resolution Imaging Spectroradiometer, Rocky Mountains, USA, Journal of Geophysical Research: Biogeosciences, 118, 1461-1471, 10.1002/jgrg.20120, 2013.

Wang, H., and Su, W.: Evaluating and understanding top of the atmosphere cloud radiative effects in Intergovernmental Panel on Climate Change (IPCC) Fifth Assessment Report (AR5) Coupled Model Intercomparison Project Phase 5 (CMIP5) models using satellite observations, Journal of Geophysical Research: Atmospheres, 118, 683-699, doi:10.1029/2012JD018619, 2013.

Winton, M.: Simple optical models for diagnosing surface-atmosphere shortwave interactions, Journal of Climate, 18, 3796-3806, 2005.

Winton, M.: Surface Albedo Feedback Estimates for the AR4 Climate Models, Journal of Climate, 19, 359-365, 10.1175/jcli3624.1, 2006.

Zhao, D., Xin, J., Gong, C., Wang, X., Ma, Y., and Ma, Y.: Trends of Aerosol Optical Properties over the Heavy Industrial Zone of Northeastern Asia in the Past Decade (2004–15), Journal of the Atmospheric Sciences, 75, 1741-1754, 10.1175/jas-d-17-0260.1, 2018.

**Table 1**. Definition of CERES input variables and other system optical properties derived from CERES inputs. All variables are 2001-2016 monthly means at 1° × 1° spatial resolution.

| | | |
|---|---|---|
| **CERES EBAF v.4 Shortwave Boundary Fluxes** | | |
| $SW_{\downarrow}^{TOA}$ | Downwelling solar flux at top-of-atmosphere | $Wm^{-2}$ |
| $SW_{\downarrow}^{SFC}$ | Downwelling solar flux at surface | $Wm^{-2}$ |
| $SW_{\downarrow,CLR}^{SFC}$ | Clear-sky downwelling solar flux at surface | $Wm^{-2}$ |
| $SW_{\uparrow}^{TOA}$ | Upwelling solar flux at top-of-atmosphere | $Wm^{-2}$ |
| $SW_{\uparrow}^{SFC}$ | Upwelling solar flux at surface | $Wm^{-2}$ |
| **System Optical Properties** | | |
| $T = SW_{\downarrow}^{SFC} / SW_{\downarrow}^{TOA}$ | Clearness index | unitless |
| $\alpha_p = SW_{\uparrow}^{TOA} / SW_{\downarrow}^{TOA}$ | Planetary albedo | unitless |
| $\alpha_s = SW_{\uparrow}^{SFC} / SW_{\downarrow}^{SFC}$ | Surface albedo | unitless |
| $A_p = 1 - \alpha_p$ | Effective planetary absorption | unitless |
| $A_s = \left[ SW_{\downarrow}^{SFC} - SW_{\uparrow}^{SFC} \right] / SW_{\downarrow}^{TOA}$ | Effective surface absorption | unitless |
| $A_a = A_p - A_s$ | Effective atmospheric absorption | unitless |
| $T_a = 1 - A_a$ | Effective atmospheric transmission | unitless |
| $T_{a,CLR} = 1 - A_{a,CLR}$ | Clear-sky effective atmospheric transmission | unitless |
| $\tau$ | Cloud visible optical depth | unitless |
| $c$ | Cloud area fraction | fraction |

**Table 2.** Normalized absolute deviation and CERES kernel ranking.

| | Global | | Land only | | |
|---|---|---|---|---|---|
| | *NAD* | Rank | *NAD* | Rank | Mean Rank |
| **ISO** | 0.05 | 6 | 0.05 | 6 | *6* |
| **ANISO** | 0.64 | 3 | 0.59 | 3 | *3* |
| **C12** | 0.45 | 4 | 0.47 | 4 | *4* |
| **M10** | 0.26 | 5 | 0.34 | 5 | *5* |
| **QH06** | 0.66 | 2 | 0.60 | 2 | *2* |
| **BO18** | 0.67 | 1 | 0.64 | 1 | *1* |

Geosci. Model Dev. Discuss., https://doi.org/10.5194/gmd-2019-15
Manuscript under review for journal Geosci. Model Dev.
Discussion started: 26 February 2019


Geoscientific Model Development Discussions
Open Access

**Table 3.** Global monthly mean bias (*MB*) and mean absolute bias (*MAB*) for $K_\alpha^{BO18}$ emulated with *T* and $SW_\downarrow^{SFC}$ from ECHAM6 and CAM5. For reference, the global mean value of $K_\alpha^{BO18}$ is 133 W m$^{-2}$.

MB (W m$^{-2}$)

| | **Jan.** | **Feb.** | **Mar.** | **Apr.** | **May** | **Jun.** | **Jul.** | **Aug.** | **Sep.** | **Oct.** | **Nov.** | **Dec.** | **Ann.** |
|---|---|---|---|---|---|---|---|---|---|---|---|---|---|
| $K_\alpha^{BO18} - K_\alpha^{CAM5}$ | -2.9 | -3.4 | -3.3 | -3.9 | -4.4 | -3.8 | -3.8 | -3.7 | -3.4 | -3.8 | -3.7 | -3.3 | -3.6 |
| $K_\alpha^{BO18} - K_\alpha^{ECHAM6}$ | -1.9 | -2.2 | -1.8 | -1.9 | -2.2 | -1.5 | -1.1 | -1.6 | -1.7 | -2.5 | -2.5 | -1.8 | -1.9 |

MAB (W m$^{-2}$)

| | **Jan.** | **Feb.** | **Mar.** | **Apr.** | **May** | **Jun.** | **Jul.** | **Aug.** | **Sep.** | **Oct.** | **Nov.** | **Dec.** | **Ann.** |
|---|---|---|---|---|---|---|---|---|---|---|---|---|---|
| $\lvert K_\alpha^{BO18} - K_\alpha^{CAM5} \rvert$ | 6.9 | 5.7 | 5.2 | 6.8 | 7.7 | 8.6 | 7.9 | 6.7 | 5.6 | 6.1 | 6.9 | 6.9 | 6.8 |
| $\lvert K_\alpha^{BO18} - K_\alpha^{ECHAM6} \rvert$ | 6.3 | 5.7 | 5.0 | 5.9 | 6.7 | 6.8 | 6.4 | 5.8 | 5.3 | 5.6 | 6.4 | 6.7 | 6.1 |

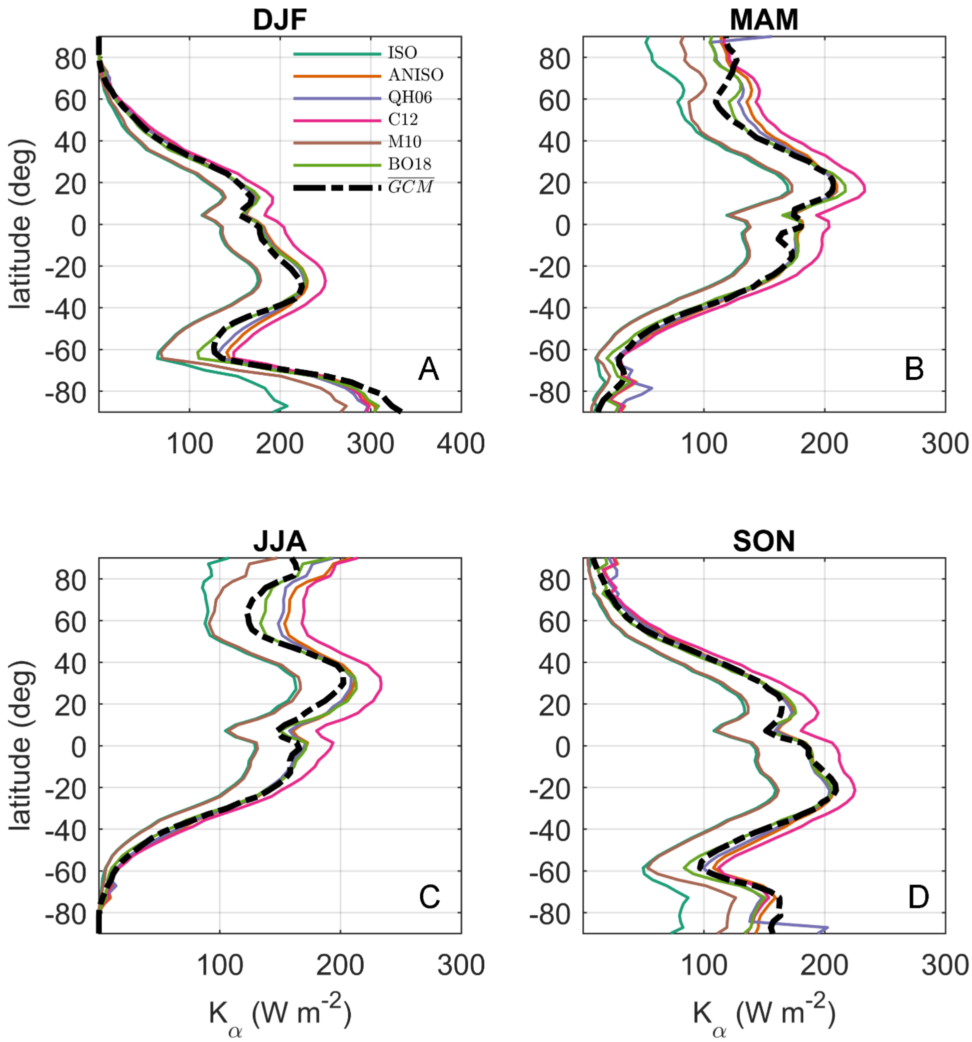


**Figure 1.** Latitudinal (1°) and seasonal means of $K_{\alpha}^{\overline{GCM}}$ and $K_{\alpha}^{CERES}$ for: A) December-January-February (DJF); B) March-April-May (MAM); C) June-July-August (JJA); D) September-October-November (SON).

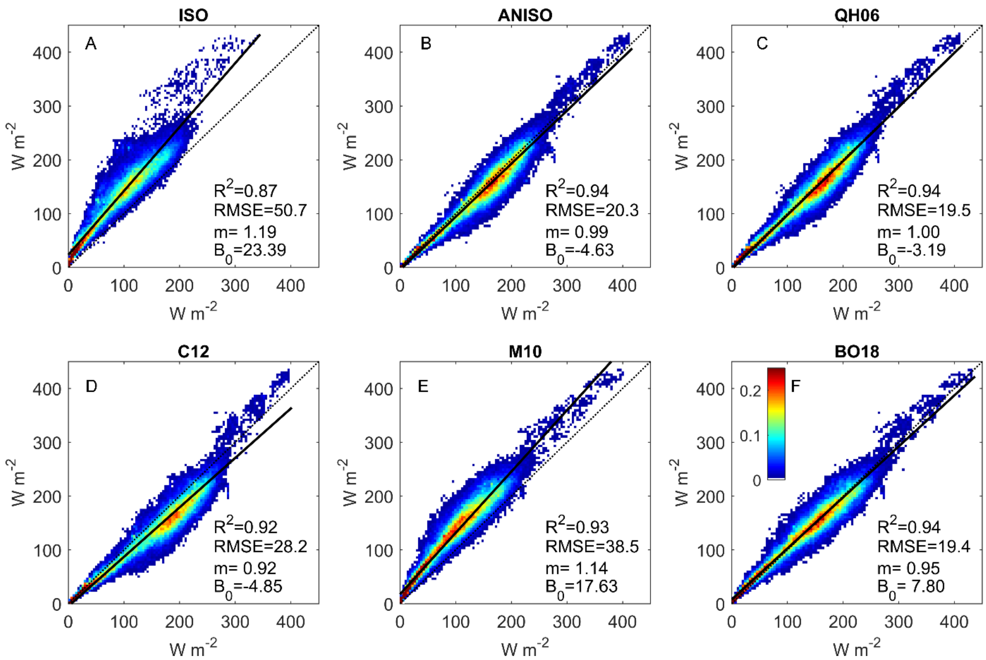


**Figure 2.** A)-F): Scatter-density regressions of global monthly mean $K_\alpha^{\overline{GCM}}$ (y-axis) and $K_\alpha^{CERES}$ (x-axis), with the CERES kernel identifier shown at the top of each sub-panel. "*m*" = slope; "$B_0$" = y-intercept. The color scale indicates the percentage of regression points that fall within a 100 × 100 sample grid centered on the plotted point.

Geosci. Model Dev. Discuss., https://doi.org/10.5194/gmd-2019-15
Manuscript under review for journal Geosci. Model Dev.
Discussion started: 26 February 2019


Geoscientific Model Development Discussions
Open Access
EGU

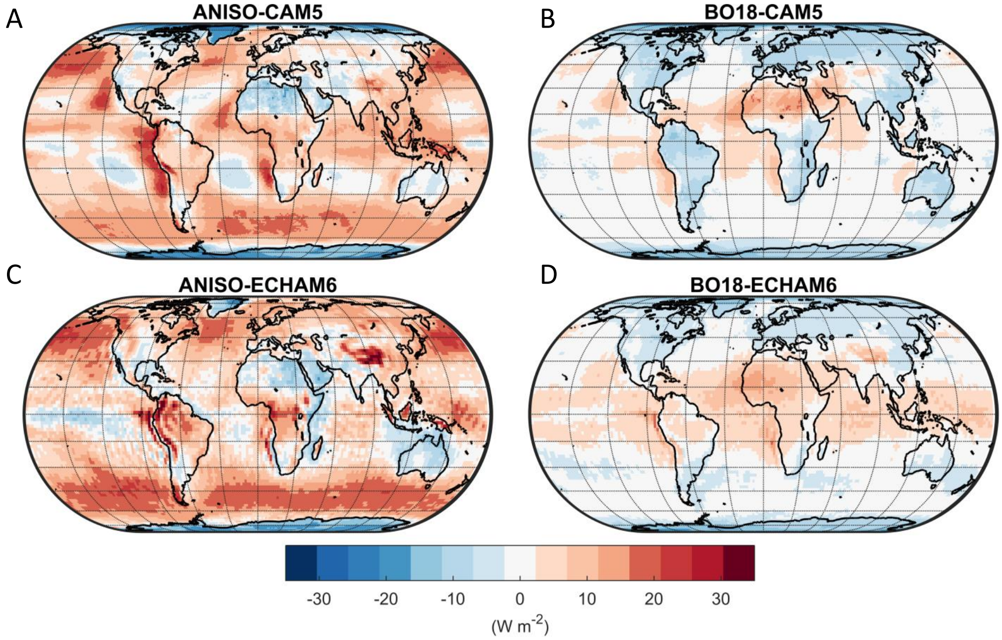


**Figure 3.** A) Mean annual bias of the CAM5 albedo change kernel emulated with the ANISO analytical model; B) Mean annual bias of the CAM5 albedo change kernel emulated with the BO18 parameterization; C) Mean annual bias of the ECHAM6 albedo change kernel emulated with the ANISO analytical model; D) Mean annual bias of the ECHAM6 albedo change kernel emulated with the BO18 parameterization

Geosci. Model Dev. Discuss., https://doi.org/10.5194/gmd-2019-15
Manuscript under review for journal Geosci. Model Dev.
Discussion started: 26 February 2019

Geoscientific Model Development
Discussions
Open Access

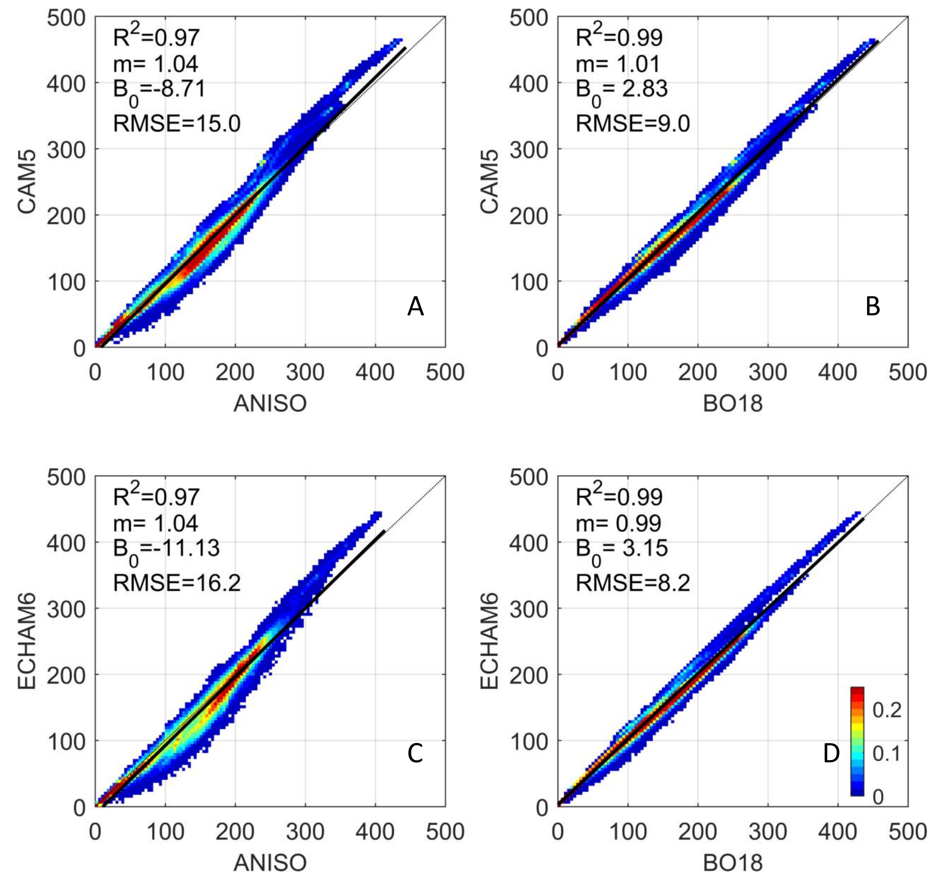


**Figure 4.** A)-D): Scatter-density regressions of $K_\alpha^{GCM}$ (y-axis) and $K_\alpha^{GCM}$ emulated with the ANISO model and BO18 parameterization (x-axis); "*m*" = slope; "$B_0$" = y-intercept. The color scale indicates the percentage of regression points that fall within a 100 × 100 sample grid centered on the plotted point.